Generic low-density corrections to the equation of state of chain molecules with repulsive intermolecular forces

van Westen, Thijs; Rehner, Philipp; Vlugt, Thijs J.H.; Gross, Joachim

DOI
10.1063/5.0197910

Publication date
2024

Document Version
Final published version

Published in
Journal of Chemical Physics

The Journal of Chemical Physics ARTICLE pubs.aip.org/aip/jcp

Generic low-density corrections to the equation of state of chain molecules with repulsive intermolecular forces

Cite as: J. Chem. Phys. 160, 174105 (2024); doi: 10.1063/5.0197910
Submitted: 15 January 2024 • Accepted: 16 April 2024 •
Published Online: 1 May 2024

Thijs van Westen,[1,a)] Philipp Rehner,[2] Thijs J. H. Vlugt,[3] and Joachim Gross[1,a)]

AFFILIATIONS

[1] Institute of Thermodynamics and Thermal Process Engineering, University of Stuttgart, Pfaffenwaldring 9, D-70569 Stuttgart, Germany
[2] Energy and Process Systems Engineering, Department of Mechanical and Process Engineering, ETH Zurich, Tannenstrasse 3, 8092 Zurich, Switzerland
[3] Engineering Thermodynamics, Process & Energy Department, Faculty of Mechanical, Maritime and Materials Engineering, Delft University of Technology, Leeghwaterstraat 39, Delft 2628CB, The Netherlands

[a)] **Authors to whom correspondence should be addressed:** thijs.van-westen@itt.uni-stuttgart.de and gross@itt.uni-stuttgart.de

ABSTRACT

Molecular-based equations of state for describing the thermodynamics of chain molecules are often based on mean-field like arguments that reduce the problem of describing the interactions between chains to a simpler one involving only nonbonded monomers. While for dense liquids such arguments are known to work well, at low density they are typically less appropriate due to an incomplete description of the effect of chain connectivity on the local environment of the chains' monomer segments. To address this issue, we develop three semi-empirical approaches that significantly improve the thermodynamic description of chain molecules at low density. The approaches are developed for chain molecules with repulsive intermolecular forces; therefore, they could be used as reference models for developing equations of the state of real fluids based on perturbation theory. All three approaches are extensions of Wertheim's first-order thermodynamic perturbation theory (TPT1) for polymerization. The first model, referred to as TPT1-v, incorporates a second-virial correction that is scaled to zero at liquid-like densities. The second model, referred to as TPT1-y, introduces a Helmholtz-energy contribution to account for correlations between next-nearest-neighbor segments within chain molecules. The third approach, called TPT-E, directly modifies TPT1 without utilizing an additional Helmholtz energy contribution. By employing TPT1 at the core of these approaches, we ensure an accurate description of mixtures and enable a seamless extension from chains of tangentially bonded hard-sphere segments of equal size to hetero-segmented chains, fused chains, and chains of soft repulsive segments (which are influenced by temperature). The low-density corrections implemented in TPT1 are designed to preserve these good characteristics, as confirmed through comparisons with novel molecular simulation results for the pressure of various chain fluids. TPT1-v exhibits excellent transferability across different chain types, but it relies on knowing the second virial coefficient of the chain molecules, which is non-trivial to obtain and determined here using Monte Carlo simulation. The TPT1-y model, on the other hand, achieves comparable accuracy to TPT1-v while being fully predictive, requiring no input besides the geometry of the chain molecules.

I. INTRODUCTION

Equations of state for describing fluids containing polyatomic (chain) molecules are important for the design of processes and products in the (petro-)chemical, energy, and pharmaceutical industries. Models derived from a description of molecules and their interactions have proven particularly useful, providing a unique combination of accuracy and predictive power. A well-established approach for developing such molecular-based equation-of-state models is to start from a reference molecular model comprising only repulsive intermolecular forces and later incorporate the effects of attractive intermolecular interactions (such as dispersion, polarity, or hydrogen bonding) as perturbations. Notable examples of successful equations of state for chain molecules developed this way are the perturbed hard-chain theory (PHCT) of Beret, Donohue, and Prausnitz,[1,2] as well as the Statistical Associating Fluid

Theory (SAFT) family of models,[3–9] which have found extensive applications in describing the thermodynamic properties and phase behavior of systems ranging from mixtures of *n*-alkanes to polymer blends, polymers in solution, and surfactants.[10–14]

One of the archetype molecular models for describing chain molecules is a fully flexible chain of tangentially bonded hard spheres, which serves as the reference model for the PHCT theory, the original SAFT models,[3–5] and the PC-SAFT equation of state.[7] Chains of hard spheres comprise some of the most essential features of chain molecules, such as excluded volume interactions, molecular anisotropy, and, depending on the way the spheres are bonded, intramolecular flexibility. Because of this, they have been intensively studied over the past 50 years, leading to equations of state based on integral equation theory (e.g., PRISM,[15] Percus Yevick theory,[16–18] Wertheim's multi-density Ornstein–Zernicke equation,[19–21] GBY hierarchy,[22,23] and Kirkwood hierarchy[24]), Wertheim's thermodynamic perturbation theory of polymerization (TPT) and its extensions,[4,25–37] Zhou and Stell's solvation theory,[38–41] generalized Flory–dimer theory (GFD),[42–50] and scaled particle theory.[51,52]

Central to the description of chain molecules within the SAFT framework is Wertheim's TPT,[25,26] which characterizes how monomers associate through strong, short-range directional attractions. In the limit of infinite association strength, Wertheim's approach provides the means to approximate the change in Helmholtz energy due to the formation of chains, using only the properties of a reference fluid of unbonded monomers as input.[4] This offers a versatile approach that can be applied to homo-segmented chains, hetero-segmented chains,[32,33,53,54] branched chains,[27,28,34,55] fused chains,[51,52,56–61] and mixtures thereof, as long as an accurate description of the thermodynamics and structure of the monomeric reference fluid (mixture) is available.

Although widely applied, TPT is not without limitations. As its main approximation, it describes the Helmholtz energy of chain formation based on that of a single chain in a fluid of monomers. Within this "single-chain approximation," the theory thus only incorporates the effect of intramolecular correlations on the equation of state of chain molecules; the effect of chain-connectivity on the correlations between the segments of different chains is neglected. At first-order (TPT1),[25] only correlations between neighboring segments within chain molecules are incorporated, while higher-order versions of the theory also incorporate intramolecular correlations between triplets (TPT2),[26,27,62] quadruplets (TPT3),[35] and so on. For isotropic (liquid or gaseous) fluids at high densities, the single-chain approximation is very reasonable because the local density around a segment of a chain molecule is similar to the local density around unbonded monomers.[63] At low densities, however, the chain connectivity significantly alters the local density around chain segments,[63,64] and the accuracy of TPT decreases substantially.[35,37]

Several studies have focused on improving the low-density behavior of TPT, ranging from fundamental approaches (e.g., changing the reference fluid to a fluid of dimers or *n*-mers,[29,30,65] or going beyond the single-chain approximation by including chain–chain interactions in Wertheim's cluster expansion[37]) to more empirical approaches where the low-density behavior is imposed.[36,41,66] The present work falls within the latter category.

Key to this work is our focus on transferability: we aim to develop low-density corrections to TPT1 that can be applied beyond chains of tangentially bonded hard spheres of equal size. That is, hetero-segmented chains, fused chains, mixtures, and soft repulsive chains. We approach this from three different angles, leading to three distinct models. The first model (TPT-v) resembles the low-density corrections proposed by Yethiraj *et al.*[67] and Vega *et al.*,[66] where the second virial coefficient predicted by TPT1 (or GFD) is replaced by the second virial coefficient obtained from Monte Carlo simulation. We scale the second-virial correction to zero when density increases, leading to an approach that bears some similarity to the recent uf-theory[68] and uv-theory.[69] The applied scaling function inherently leads to a modification of higher $(n > 2)$ virial coefficients B_n; the implications of this will be discussed and analyzed. The second model (TPT-y) draws inspiration from the work of Hu *et al.*,[39] who suggested considering correlations between neighbor- and next-nearest-neighbor segments within chain molecules to describe the Helmholtz energy of chain formation. We derive a novel approach for calculating the next-nearest-neighbor contribution, which is used as a low-density correction to TPT1. The third model (TPT-E) builds on a recent approach by Elliott,[70] where TPT1 is empirically reformulated to reproduce the correct polymer scaling of the second virial coefficient with the number of spherical segments per chain molecule.

II. THEORY DEVELOPMENT

We consider a fluid mixture of $N = N_1 + N_2 + \cdots + N_C$ chains (where C is the number of species) of arbitrarily sized, fused hard spheres in a volume V. The density of the system is defined as $\rho = N/V = \sum_{i=1}^{C} x_i \rho$, where we introduced the mole fraction of species i, $x_i = N_i/N$. Chains of species i are defined by their number of hard-sphere segments s_i, the diameters d_{α_i} of the hard spheres, and the bond lengths $l_{\alpha_i \alpha_i'}$ (which are fixed), where the index α_i runs over all segments $1, 2, \ldots, s_i$ within the chain, and the index α_i' runs over all neighbors of segment α_i. We further introduce a dimensionless bond-length $l^*_{\alpha_i \alpha_i'} = 2 l_{\alpha_i \alpha_i'} / (d_{\alpha_i} + d_{\alpha_i'})$, and the average number of hard-sphere segments per chain molecule $\bar{s} = \sum_{i=1}^{C} x_i s_i$. All chains considered in this work have no bond-bending or torsion interactions; therefore, they are free to adopt any chain conformation under the constraint that any pair of non-neighboring segments (e.g., segments 1 and 3) may only overlap if this overlap occurs within the segments that connect them along the chain's backbone (segment 2 in our example). Given the absence of bond-bending or torsion, we refer to these chains as "fully flexible," although we emphasize that increasingly fused chains effectively become more rigid due to the aforementioned constraint.

A. TPT1 for mixtures of fused, hetero-segmented hard chains

To describe fused, hetero-segmented chains of hard spheres using TPT1, we follow the recent approach of Rehner *et al.*,[61] where chains are cut into hard-sphere fragments as illustrated in Fig. 1. The dimensionless Helmholtz energy per molecule $\tilde{a} \equiv A/Nk_BT$ is described by a monomer term, defining the system of unbonded

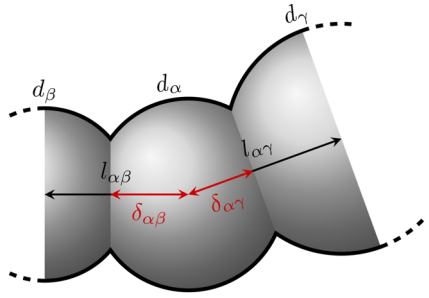

FIG. 1. Geometry of segment α fused with its neighbors $\alpha' \in \{\beta, \gamma\}$. Subscripts i have been dropped for clarity.

hard-sphere fragments, and a chain contribution for connecting the hard-sphere fragments to form chains, according to

$$\tilde{a}^{\text{TPT1}} = \bar{s}\tilde{a}^{\text{mono}} - \frac{1}{2}\sum_{i=1}^{C} x_i \sum_{\alpha_i=1}^{s_i} \sum_{\alpha_i'} \ln y^{\text{mono}}(l_{\alpha_i\alpha_i'}). \tag{1}$$

For chains of tangentially bonded monomers (no fusing), the quantity $y^{\text{mono}}(l_{\alpha_i\alpha_i'})$ is the cavity-correlation function of two hard-spheres at contact. For fused chains, it denotes an *effective* cavity-correlation function of two hard-sphere *fragments*, to be defined below.

The monomer contribution to the Helmholtz energy is calculated accurately using the Boublik–Mansoori–Carnahan–Starling–Leland (BMCSL) EoS for additive hard-sphere mixtures,[71,72]

$$\tilde{a}^{\text{mono}} = \frac{1}{\zeta_0}\left[\frac{3\zeta_1\zeta_2}{1-\zeta_3} + \frac{\zeta_2^3}{\zeta_3(1-\zeta_3)^2} + \left(\frac{\zeta_2^3}{\zeta_3^2} - \zeta_0\right)\ln(1-\zeta_3)\right], \tag{2}$$

but with the scaled-particle-theory variables $\zeta_i = \rho z_i$ modified according to the fundamental measures of the cut hard-sphere fragments,

$$z_0 = \frac{\pi}{6}\sum_{i=1}^{C} x_i \sum_{\alpha_i=1}^{s_i} = \frac{\pi}{6}\bar{s}, \tag{3}$$

$$z_1 = \frac{\pi}{6}\sum_{i=1}^{C} x_i \sum_{\alpha_i=1}^{s_i} A^*_{\alpha_i} d_{\alpha_i}, \tag{4}$$

$$z_2 = \frac{\pi}{6}\sum_{i=1}^{C} x_i \sum_{\alpha_i=1}^{s_i} A^*_{\alpha_i} d^2_{\alpha_i}, \tag{5}$$

$$z_3 = \frac{\pi}{6}\sum_{i=1}^{C} x_i \sum_{\alpha_i=1}^{s_i} V^*_{\alpha_i} d^3_{\alpha_i}, \tag{6}$$

where z_3 is the average molecular volume of the mixture, and $\zeta_3 = \eta$ is the packing fraction of the system. The quantities $A^*_{\alpha_i}$ and $V^*_{\alpha_i}$ define the ratio of the surface area and volume of a hard-sphere fragment to that of the full hard sphere, according to

$$A^*_{\alpha_i} = 1 - \frac{1}{2}\sum_{\alpha_i'}\left(1 - 2\frac{\delta_{\alpha_i\alpha_i'}}{d_{\alpha_i}}\right), \tag{7}$$

$$V^*_{\alpha_i} = 1 - \frac{1}{2}\sum_{\alpha_i'}\left[1 - 3\frac{\delta_{\alpha_i\alpha_i'}}{d_{\alpha_i}} + 4\left(\frac{\delta_{\alpha_i\alpha_i'}}{d_{\alpha_i}}\right)^3\right], \tag{8}$$

where

$$\delta_{\alpha_i\alpha_i'} = \frac{d^2_{\alpha_i} - d^2_{\alpha_i'} + 4l^2_{\alpha_i\alpha_i'}}{8l_{\alpha_i\alpha_i'}}, \tag{9}$$

defines that part of the bond-length $l_{\alpha_i\alpha_i'}$ that lays inside segment α_i (see Fig. 1). In the limit of chains of tangentially bonded hard spheres, $A^*_{\alpha_i} = V^*_{\alpha_i} = 1$, and the unmodified BMCSL EoS is recovered.

The effective cavity-correlation function of two hard-sphere fragments is described using the same functional form as the BMCSL result for the contact value of the cavity-correlation function of hard spheres,

$$y^{\text{HS}}\left(\frac{d_{\alpha_i} + d_{\alpha_i'}}{2}\right) = \frac{1}{1-\zeta_3} + \left(\frac{d_{\alpha_i} d_{\alpha_i'}}{d_{\alpha_i} + d_{\alpha_i'}}\right)\frac{3\zeta_2}{(1-\zeta_3)^2} + \left(\frac{d_{\alpha_i} d_{\alpha_i'}}{d_{\alpha_i} + d_{\alpha_i'}}\right)^2 \frac{2\zeta_2^2}{(1-\zeta_3)^3}, \tag{10}$$

but with the fundamental measures z_i calculated by Eqs. (3)–(6) and the diameters d_{α_i} and $d_{\alpha_i'}$ replaced by $l_{\alpha_i\alpha_i'} + (d_{\alpha_i} - d_{\alpha_i'})/2$ and $l_{\alpha_i\alpha_i'} + (d_{\alpha_i'} - d_{\alpha_i})/2$, leading to

$$y^{\text{mono}}(l_{\alpha_i\alpha_i'}) = \frac{1}{1-\zeta_3} + \frac{3b_{\alpha_i\alpha_i'}\zeta_2}{2(1-\zeta_3)^2} + \frac{(b_{\alpha_i\alpha_i'}\zeta_2)^2}{2(1-\zeta_3)^3}, \tag{11}$$

with the "bond function,"

$$b_{\alpha_i\alpha_i'} = \max\left(\frac{4l^2_{\alpha_i\alpha_i'} - (d_{\alpha_i} - d_{\alpha_i'})^2}{4l_{\alpha_i\alpha_i'}}, 0\right). \tag{12}$$

The bond function provides a convenient substitute for the bond length in cases where chains are hetero-segmented: it equals zero for bond-lengths that lead to total fusion of segments α and α' and reduces to $2d_\alpha d_{\alpha'}/(d_\alpha + d_\alpha)$ for tangent chains, thereby recovering the desired BMCSL result of Eq. (10) when substituted in Eq. (11). As shown by Rehner *et al.*,[61] a bond function equal to zero leads to the correct limiting behavior of Eqs. (2)–(12) for totally fused homo-segmented hard chains (i.e., a hard-sphere fluid).

B. Analysis of TPT1 prediction for the second virial coefficient

The TPT1 result for the second virial coefficient $\tilde{B}_2 \equiv (\partial\tilde{a}/\partial\rho)_{T,\rho=0}$ of a mixture of fused hetero-segmented hard chain molecules is obtained from Eqs. (1)–(9), (11), and (12) as

$$\tilde{B}_2^{\text{TPT1}} = \bar{s}\left(z_3 + 3\frac{z_1 z_2}{z_0}\right) - \frac{1}{2}\sum_{i=1}^{C} x_i \sum_{\alpha_i=1}^{s_i} \sum_{\alpha_i'} \left(z_3 + \frac{3}{2}z_2 b_{\alpha_i\alpha_i'}\right), \tag{13}$$

where the bar in $\tilde{B}_2$ denotes it is a mixture property.

For pure, homo-segmented chains, Eq. (13) simplifies as

$$\frac{B_2^{\text{TPT1}}}{(\pi/6)d^3} = 4 + (s-1)\left[6l^* - \frac{1}{2}l^{*3}\right] + (s-1)^2\left[\frac{3}{4}\left(l^{*2} + l^{*4}\right)\right]. \tag{14}$$

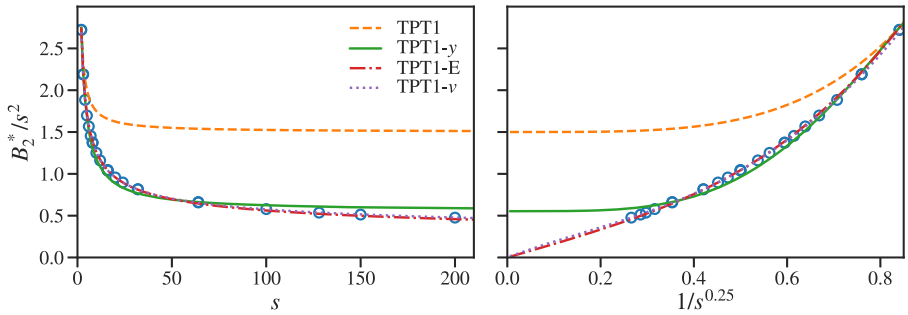

FIG. 2. Second virial coefficient of homo-segmented tangent hard-sphere chains: $B_2^* = B_2/((\pi/6)d^3)$. A comparison between the results of TPT1, TPT1-y, TPT1-E, and TPT1-v to the results obtained from MC simulation (symbols).[66,67,73]

In Fig. 2, the results of this equation are compared to MC simulation data[66,67,73] for the second virial coefficient of tangent hard-sphere chains ($l^* = 1$). The rather large overestimation of B_2 for longer chains is a known effect and is rooted in the single-chain approximation underlying TPT,[35,37,74] which leads to a too strong asymptotic (polymer) scaling, $B_2^{\mathrm{TPT1}} \sim s^2$, as compared to the scaling implied by MC simulations, $B_2 \sim s^{2-\nu}$ with $\nu \approx 0.25$.[67] We exemplify this in the right diagram of Fig. 2, where we plot B_2^*/s^2 vs $s^{-\nu}$. For the longer chains shown, the MC simulation results for B_2^*/s^2 depend linearly on $s^{-\nu}$, while the TPT1 result approaches a constant positive value.

Interestingly, the asymptotic scaling $B_2^{\mathrm{TPT1}} \sim s^2$ is correct for chains comprising segments fixed in a rigid, linear configuration.[75,76] Fusing the segments of flexible chains effectively increases the chains' rigidity because next-to-nearest neighbor segments α and α'' are not allowed to overlap outside the middle segment α' of the respective triplet (see Fig. 3, $\alpha\alpha'\alpha'' \to \alpha\beta\gamma$). This suggests that the second virial coefficient predicted by TPT1 is more appropriate for fused chains than for tangent chains.

C. TPT1-v

As a first approach to improve the TPT1 description of chain fluids at low densities, we add a correction term that replaces the second virial coefficient predicted by TPT1 with the actual, smaller second virial coefficient of the chain fluid. Since TPT1 is known to provide an accurate description of high-density chain fluids, we scale down the correction term for increasing packing fraction η. We find that a simple exponential scaling with packing fraction leads to good results,

$$\tilde{a}^{\,\mathrm{TPT1}-v} = \tilde{a}^{\,\mathrm{TPT1}} + \exp(-\eta)\left(\tilde{B}_2 - \tilde{B}_2^{\mathrm{TPT1}}\right)\rho, \tag{15}$$

where

$$\tilde{B}_2 = \sum_{i=1}^{C}\sum_{j=1}^{C} x_i x_j B_{2,ij}, \tag{16}$$

with $B_{2,ij}$ being the second virial coefficient of species i and j.

For pure, fully flexible homo-segmented tangent hard-sphere chains, the second virial coefficient required by Eq. (15) is calculated using an analytic model developed in Appendix A. The second virial coefficients describing fused chains, hetero-chains, or cross interactions in mixtures are for now calculated based on MC simulations (see Appendix E for the simulation details and Table I for the results); the development of an analytic model for the second virial coefficient of such chain molecules may be the subject of subsequent work.

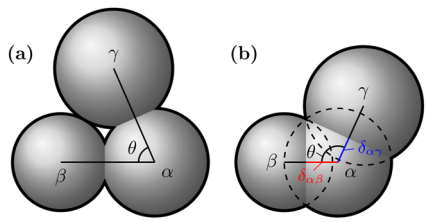

FIG. 3. Schematic showing that the minimum allowed bond-angle θ increases for more strongly fused triplets. Effectively, the more strongly fused triplet in (b) is more rigid.

TABLE I. Second virial coefficient of two fully flexible chains of s (fused) hard-sphere segments was obtained from MC simulation. The estimated statistical uncertainty of the last digit is given in parentheses. Comparison of block-copolymers (A–A–B–B), alternating chains (A–B–A–B), mixtures (A–A–A–A + B–B–B–B), and homo-segmented chains (C–C–C–C) of equal average segment volume $(\pi/6)d_{12}^3 \equiv (\pi/6)(s_1+s_2)^{-1}\sum_{i=1}^{2}\sum_{\alpha_i} d_{\alpha_i}^3$.

d_{12}^3	s	l^*	d_A	d_B	Chain 1	Chain 2	B_2
1.872	10	1	1	1.4	A–A–B–B	A–A–B–B	118.61(1)
1.872	10	1	1	1.4	A–B–A–B	A–B–A–B	118.63(2)
1.872	10	0.8	1	1.4	A–B–A–B	A–B–A–B	91.39(2)
1.872	10	0.6	1	1.4	A–B–A–B	A–B–A–B	70.83(4)
1.872	10	1	1	1.4	A–A–A–A	B–B–B–B	111.08(8)
1.872	10	1	d_{12}	d_{12}	C–C–C–C	C–C–C–C	122.9969[a]
1.476 55	20	1	1	1.25	A–A–B–B	A–A–B–B	292.0(1)
1.476 55	20	1	1	1.25	A–B–A–B	A–B–A–B	292.3(1)
1.476 55	20	1	d_{12}	d_{12}	C–C–C–C	C–C–C–C	296.2788[a]

[a]Model from Eqs. (A1) and (A2).

We emphasize that Eq. (15) exactly reproduces the second virial coefficient B_2 that is given as input. If the model for B_2 has the proper asymptotic scaling with the number of segments s, the TPT-υ model thus reproduces this scaling.

D. TPT1-y

As another approach to improve the TPT1 description of chain fluids at low densities, we follow a route similar to that taken by Hu, Liu, and Prausnitz.[39,40] Central to this approach is Zhou and Stell's "zero-order approximation" for chemical association of sticky spheres into chains,[38] which relates the Helmholtz energy of chain formation to the s-particle cavity-correlation function of a fluid of non-bonded monomers $y^{(s)}(1,2,\ldots,s)$, where $(1,2,\ldots,s)$ is a configuration of s monomers that yields the structure of a fully bonded chain molecule,

$$\tilde{a} = \bar{s}\tilde{a}^{\text{mono}} - \sum_i x_i \ln y_i^{(s_i)}(1,2,\ldots,s_i). \tag{17}$$

Following Hu, Liu, and Prausnitz, we approximate the cavity-correlation function as a product of correlations between neighbors $(\alpha\alpha')$ and next-nearest neighbors $(\alpha\alpha'')$ within a chain,

$$y_i^{(s_i)}(1,2,\ldots,s_i) \approx \left(\prod_{\alpha_i=1}^{s_i} \prod_{\alpha_i'} y_{i,\alpha_i\alpha_i'}^{(2)} \prod_{\alpha_i=1}^{s_i} \prod_{\alpha_i''} y_{i,\alpha_i\alpha_i''}^{(2)} \right)^{1/2}, \tag{18}$$

where the square-root is to prevent overcounting. Substituting Eq. (18) into Eq. (17), one obtains

$$\tilde{a} = \bar{s}\tilde{a}^{\text{mono}} - \frac{1}{2}\sum_{i=1}^{C} x_i \left[\sum_{\alpha_i=1}^{s_i} \sum_{\alpha_i'} \ln y_{i,\alpha_i\alpha_i'}^{(2)} + \sum_{\alpha_i=1}^{s_i} \sum_{\alpha_i''} \ln y_{i,\alpha_i\alpha_i''}^{(2)} \right]. \tag{19}$$

Contrary to the approach of Hu, Liu, and Prausnitz, where both the nearest- and next-nearest neighbor contributions of Eq. (19) are described based on empirical functions correlated to molecular simulation data, we only use an empirical equation for describing the next-nearest-neighbor contribution—for describing the nearest-neighbor contribution, we simply adopt the TPT1 expression of Sec. II A. The description of tangent hard-sphere dimers thereby remains practically unaltered as compared to the approach of Hu, Liu, and Prausnitz (in fact, it improves slightly), but, given the generic nature of the TPT1 of Sec. II A, the benefits of describing fused chains, hetero-chains, and mixtures are substantial.

The basic equation of our model, referred to as TPT1-y, follows as

$$\tilde{a}^{\text{TPT1}-y} = \tilde{a}^{\text{TPT1}} - \frac{1}{2}\sum_{i=1}^{C} x_i \sum_{\alpha_i=1}^{s_i} \sum_{\alpha_i''} \ln y_{i,\alpha_i\alpha_i''}^{(2)}. \tag{20}$$

The remainder of this section is devoted to developing an empirical function for the effective cavity-correlation function of next-nearest neighbor segments $\ln y_{i,\alpha_i\alpha_i''}^{(2)}$. With the aim of preserving the generic nature of the TPT1 described in Sec. II A, we take inspiration from the (effective) cavity-correlation function of nearest-neighbor segments of Eqs. (11) and (12).

For now, we will drop the subscript i that denotes the species type. Let us first propose a bond function $b_{\alpha\alpha''}$ for next-nearest neighbor segments α and α'' based on the bond function $b_{\alpha\alpha'}$ of neighboring segments α and α' from Eq. (12). The bond function of next-nearest neighbors should be zero in case there is no $\alpha\alpha''$ interaction; this happens when (1) the outer segments α and/or α'' are completely contained within the middle segment α', or (2) when the outer segments are completely contained within each other. Since the outer segments may only overlap with each other *within* the middle segment α', case (1) encompasses case (2). For all other cases, we assume the bond function can be described by a characteristic distance $L_{\alpha\alpha''}$, leading to the following definition:

$$b_{\alpha\alpha''} = \begin{cases} 0 & \text{if } l_{\alpha'\alpha''} < \frac{1}{2}(d_{\alpha'} - d_{\alpha''}), \\ 0 & \text{if } l_{\alpha\alpha'} < \frac{1}{2}(d_{\alpha'} - d_{\alpha}), \\ L_{\alpha\alpha''}, & \text{otherwise}. \end{cases} \tag{21}$$

We define the characteristic length $L_{\alpha\alpha''}$ in terms of the averaged squared distance between segments α and α'' (which can be obtained from the cosine rule), leading to

$$L_{\alpha\alpha''}^2 \equiv \left\langle r_{\alpha\alpha''}^2 \right\rangle_{\boldsymbol{\omega}} = l_{\alpha\alpha'}^2 + l_{\alpha'\alpha''}^2 - 2 l_{\alpha\alpha'} l_{\alpha'\alpha''} \langle \cos\theta \rangle_{\boldsymbol{\omega}}, \tag{22}$$

where $r_{\alpha\alpha''} = |\boldsymbol{r}_\alpha - \boldsymbol{r}_{\alpha''}|$ is the distance between segments α and α'', $\boldsymbol{\omega}_1 = \hat{\boldsymbol{r}}_\alpha - \hat{\boldsymbol{r}}_{\alpha'}$ and $\boldsymbol{\omega}_2 = \hat{\boldsymbol{r}}_{\alpha''} - \hat{\boldsymbol{r}}_{\alpha'}$ denote the orientation vectors of the two bonds (the hat denotes a unit vector), and $\theta = \arccos(\boldsymbol{\omega}_1 \cdot \boldsymbol{\omega}_2)$ is the bond angle. The orientational average is solved analytically by aligning the orientation of molecule 1 with the z-axis of a Cartesian reference frame. After changing to spherical coordinates, the polar angle of molecule 2 then coincides with the bond-angle θ, and the integrations over the polar angle of molecule 1 and both azimuthal angles can be done independently. We obtain

$$\begin{aligned} \langle \cos\theta \rangle_{\boldsymbol{\omega}} &= \frac{\iint \cos\theta \, \mathrm{d}\boldsymbol{\omega}_1 \mathrm{d}\boldsymbol{\omega}_2}{\iint \mathrm{d}\boldsymbol{\omega}_1 \mathrm{d}\boldsymbol{\omega}_2} \\ &= \frac{\int_{\theta_{\min}}^{\pi} \cos\theta \sin\theta \, \mathrm{d}\theta}{\int_{\theta_{\min}}^{\pi} \sin\theta \mathrm{d}\theta} \\ &= \frac{1}{2}(\cos\theta_{\min} - 1). \end{aligned} \tag{23}$$

The minimum possible bond angle $\theta_{\min}$ for which segments α and α'' do not overlap outside the middle segment α' (see Fig. 3 for a schematic, $\alpha\alpha'\alpha'' \to \alpha\beta\gamma$) follows from the following exact result:[61]

$$\cos\theta_{\min} = \begin{cases} \dfrac{4\left(l_{\alpha\alpha'}^2 + l_{\alpha'\alpha''}^2\right) - \left(d_\alpha + d_{\alpha''}\right)^2}{8 l_{\alpha\alpha'} l_{\alpha'\alpha''}} & \text{if } \chi \geq 1, \\ \dfrac{4\delta_{\alpha'\alpha}\delta_{\alpha'\alpha''} - \sqrt{\left(d_{\alpha'}^2 - 4\delta_{\alpha'\alpha}^2\right)\left(d_{\alpha'}^2 - 4\delta_{\alpha'\alpha''}^2\right)}}{d_{\alpha'}^2} & \text{if } \chi < 1, \end{cases} \tag{24}$$

where $\delta_{\alpha'\alpha}$ and $\delta_{\alpha'\alpha''}$ are calculated using Eq. (9), and

$$\chi = 4\frac{d_\alpha l_{\alpha'\alpha''}^2 + d_{\alpha''} l_{\alpha\alpha'}^2}{d_{\alpha'}^2 (d_\alpha + d_{\alpha''})} - \frac{d_\alpha d_{\alpha''}}{d_{\alpha'}^2} \tag{25}$$

is a parameter that decreases for more fused chains; $\chi \geq 1$ and $\chi < 1$ correspond to cases (a) and (b) shown in Fig. 3, respectively. For homo-segmented chains, the minimum bond-angle simplifies to

$$\cos\theta_{\min} = \begin{cases} 1 - \frac{1}{2} l^{*-2} & \text{if } l^* \geq \frac{1}{\sqrt{2}}, \\ 2 l^{*2} - 1 & \text{if } l^* < \frac{1}{\sqrt{2}}. \end{cases} \tag{26}$$

To obtain an expression for the effective cavity-correlation function of next-nearest neighbor segments $\ln y^{(2)}_{i,\alpha_i\alpha_i''}$, we substitute the bond function $b_{\alpha_i\alpha_i''}$ of Eq. (21) for $b_{\alpha_i\alpha_i'}$ in Eq. (11) and make some empirical modifications, which will be explained below,

$$\ln y^{(2)}_{i,\alpha_i\alpha_i''} = \Theta(s_i - 2)\left(\frac{s_i - 2}{s_i}\right) b^{*\frac{3}{2}}_{\alpha_i\alpha_i''} \ln\left[1 - b^{*2}_{\alpha_i\alpha_i''} + \frac{b^{*2}_{\alpha_i\alpha_i''}}{1-\zeta_3} + \frac{a_0 b_{\alpha_i\alpha_i''}\zeta_2}{(1-\zeta_3)^2} + \frac{a_1 (b_{\alpha_i\alpha_i''}\zeta_2)^2}{(1-\zeta_3)^{\frac{1}{2}}}\right]. \tag{27}$$

When substituting this result in the next-nearest-neighbor contribution of Eq. (20), the product of the Heavyside function $\Theta(s_i - 2)$ with $(s_i - 2)/s_i$ renders a next-nearest neighbor contribution that is zero for chains with (less than) two segments and that is without discontinuities at $s_i = 2$ [note that the sum over α_i'' in Eq. (20) introduces another multiplication with $s_i - 2$]. This is useful for possible applications of the model to molecules with non-integer numbers of s_i, e.g., $1 < s_i < 2$. We further introduced

$$b^*_{\alpha_i\alpha_i''} = \frac{b_{\alpha_i\alpha_i''}}{L^{\text{tangent}}_{\alpha_i\alpha_i''}} \tag{28}$$

as a parameter that varies between zero and unity when going from a fully fused to a tangentially bonded triplet. This parameter is used to maintain the correct limit of total fusion (i.e., a hard sphere) dictated by TPT1 of Sec. II A.[61]

The empirical parameters a_0 and a_1 are given a dependence on the number of spherical segments of a chain molecule, according to

$$\begin{aligned} a_0 &= a_{00} + a_{01}\left(\frac{s_i - 2}{s_i}\right) + a_{02}\left(\frac{s_i - 2}{s_i}\right)^2, \\ a_1 &= a_{10} + a_{11}\left(\frac{s_i - 2}{s_i}\right) + a_{12}\left(\frac{s_i - 2}{s_i}\right)^2. \end{aligned} \tag{29}$$

The six adjustable model constants a_{ij} are used to correlate MC and MD simulation results[35,61,77] for the pressure of fully flexible homo-segmented tangent hard-sphere chains comprising between 3 and 500 hard-sphere segments (see the supplementary material for the complete dataset, and Table II for the correlated model constants), leading to an average absolute relative deviation (AAD) of 0.48% per datapoint and a maximum absolute relative deviation (Max-AD) of 2.8%.

We note that the modified density dependence of the last term of Eq. (27) as compared to that of Eq. (11) can be justified to some extent. Since we aim to describe the correlation between the terminal segments α and α'' of a triplet, the density dependence of Eq. (27) should be less strong than for the pair correlations between neighboring segments α and α' described by Eq. (11).[78] We find that reducing the power of the last term of Eq. (11) to a square root works well in that respect.

TABLE II. Correlated constants of Eq. (29).

a_{00}	0.357 49
a_{01}	−1.259 1
a_{02}	0.848 41
a_{10}	−1.342 0
a_{11}	3.248 7
a_{12}	−2.524 3

E. TPT1-E

As a third approach to improving the TPT1 description of chain fluids at low densities, we elaborate on a suggestion by Elliott[70] and replace the constant 3/2 appearing in the effective cavity correlation function of hard-sphere fragments of Eq. (11) by an empirical function $C(s_i, b_{\alpha_i\alpha_i'})$ that enforces the correct polymer scaling of the second virial coefficient,

$$y^{\text{mono}}(l_{\alpha_i\alpha_i'}) = \frac{1}{1-\zeta_3} + C(s_i, b_{\alpha_i\alpha_i'})\frac{b_{\alpha_i\alpha_i'}\zeta_2}{(1-\zeta_3)^2} + \frac{(b_{\alpha_i\alpha_i'}\zeta_2)^2}{2(1-\zeta_3)^3}. \tag{30}$$

The second virial coefficient corresponding to this modified TPT1 can be written as

$$\tilde{B}_2 = \tilde{s}\left(z_3 + 3\frac{z_1 z_2}{z_0}\right) - \frac{1}{2}\sum_{i=1}^{C} x_i \sum_{\alpha_i=1}^{s_i}\sum_{\alpha_i'}\left(z_3 + C(s_i, b_{\alpha_i\alpha_i'})z_2 b_{\alpha_i\alpha_i'}\right). \tag{31}$$

For tangent hard-sphere chains, the empirical function C must cancel that contribution to Eq. (31) which scales as $\sim s^2$, which is $\tilde{s}3z_1z_2/z_0$. The polymer scaling $B_2 \sim s^{2-\nu}$ (with $\nu \approx 0.25$) is then enforced using two empirical constants c_1 and c_3, according to

$$\begin{aligned} C^{\text{tangent}}(s_i, b_{\alpha_i\alpha_i'}) &= 3\frac{z_1}{z_0 b_{\alpha_i\alpha_i'}} - \frac{c_1}{\sqrt{s_i}} - \frac{c_3}{\sqrt{1+\sqrt{s_i - 1}}} \\ &\equiv \kappa(s_i) - \frac{c_3}{\sqrt{1+\sqrt{s_i-1}}}. \end{aligned} \tag{32}$$

To recover the original TPT1 in the case of a dimer, we impose the boundary condition $C(s = 2) = 3/2$, which fixes the constant c_3 as

$$c_3 = \left(\kappa(2) - \frac{3}{2}\right)\sqrt{2}. \tag{33}$$

Equations (32) and (33) essentially recover the functional form proposed by Elliott.[70] The empirical constant $c_1 = 0.5632$ was adjusted to reproduce MC simulation data for the second virial coefficient of fully flexible homo-segmented tangent hard-sphere chains[66,67,73] of three up to 200 segments (see the supplementary material for the complete dataset).

To extend these results to fused chains, we introduce the dimensionless bond function of two neighboring segments,

$$b^*_{\alpha_i\alpha_i'} \equiv \frac{b_{\alpha_i\alpha_i'}}{b^{\text{tangent}}_{\alpha_i\alpha_i'}}, \tag{34}$$

which varies conveniently from zero for a configuration where the two segments are completely fused to unity for a configuration where they are tangentially bonded. For fully fused chains ($b^*_{\alpha_i\alpha'_i} = 0$), we assume a polymer scaling consistent with that of rigid linear chains $B_2 \sim s^2$, whereas for tangent (fully flexible) chains ($b^*_{\alpha_i\alpha'_i} = 1$) Eqs. (32) and (33) should remain unaltered. For fused chains characterized by $0 < b^*_{\alpha_i\alpha'_i} < 1$, we interpolate between these two limits using an empirical parameter c_2. We propose

$$C(s_i, b_{\alpha_i\alpha'_i}) = b^*_{\alpha_i\alpha'_i}\kappa(s_i) - \frac{\left(b^*_{\alpha_i\alpha'_i}\kappa(2) - \frac{3}{2}\right)\sqrt{2}}{\sqrt{1 + (s_i - 1)^{\xi}}}, \tag{35}$$

with

$$\xi = c_2 b^*_{\alpha_i\alpha'_i} + (2\nu - c_2) b^{*2}_{\alpha_i\alpha'_i} \begin{cases} 2\nu & b^*_{\alpha_i\alpha'_i} = 1, \\ 0 & b^*_{\alpha_i\alpha'_i} = 0. \end{cases} \tag{36}$$

The constant $c_2 = 1.239$ was fitted to MC simulation data for the pressure of homo-segmented fused hard-sphere chains of 20 segments (see the supplementary material for MC data).

We note that the imposed scaling of rigid linear chains $B_2 \sim s^2$ for $b^* \to 0$ does not do justice to the fact that very long polymers might well be flexible on the scale of the contour length L of the full polymer, even if they are strongly fused.[79–81] In other words, the flexibility of a polymer does not depend solely on the local stiffness (as measured by the persistence length L_p) but also on the number of segments s. It would be interesting to analyze if and how the number of Kuhn segments[79,81] $L/(2L_p)$ could be used to replace the dimensionless bond-function b^* in the above analysis, but we consider this outside the scope of this work.

F. Extension to chains of soft repulsive segments

EOS models for real fluid mixtures are often rooted in perturbation theory, where the effect of attractive interactions between molecules (or their atoms/segments) is described as a perturbation to a reference fluid with only repulsive intermolecular interactions. A common reference fluid used in perturbation theories such as SAFT is a fluid of chain molecules with segments that interact with the positive part of the Lennard-Jones potential, a model that was first suggested by Barker and Henderson.[82] Here, we apply the TPT1-v and TPT1-y models, derived in Secs. II C–II E, to chains of spherical "Barker–Henderson" (BH) segments. For reasons discussed below, the TPT1-E model of Sec. II E leads to an equivalent description of BH chains as TPT1; therefore, this model is not analyzed further. We fix the bond-length of the molecules at the distance $l = \sigma$, where the LJ potential equals zero. Note that "tangent" in Eq. (28) now refers to chains with segments bonded at distance $l = \sigma$; therefore, $b^*_{\alpha\alpha''} = 1$ for BH chains.

As a leading-order approximation, the effect of the soft repulsive interactions between BH chains can be described by modeling the spherical segments of the chains as hard spheres of effective, temperature-dependent diameter,[83]

$$d(T) = \left(3\int_0^{\sigma}\left[1 - \exp\left(-\beta u^{\mathrm{LJ}}(r)\right)\right]r^2 \mathrm{d}r\right)^{1/3}, \tag{37}$$

where $u^{\mathrm{LJ}}(r)$ is the intermolecular potential of two LJ monomers separated by a distance r. This equation can be derived by mapping the second virial coefficient of BH monomers onto that of hard spheres: $B_2^{\mathrm{BH}} = B_{2,d}^{\mathrm{HS}} = (2/3)\pi d(T)^3$. The integral in Eq. (37) is calculated analytically;[84] the respective equations are listed in Appendix B.

It is important to note that the bond-length of the molecules is fixed at $l = \sigma$, while $d(T) \leq \sigma$. The cavity-correlation function of hard spheres that is required to evaluate the TPT1 contribution to chain formation in Eq. (1) must thus be evaluated for two hard spheres at a relative distance larger than d. We, therefore, replace Eq. (11) with the Modified Scaled Particle Theory (MSPT) model of Boublik,[85]

$$y_d^{\mathrm{hs}}(\sigma) = \exp\left(k_0 + k_1\left(\frac{\sigma}{d}\right) + k_2\left(\frac{\sigma}{d}\right)^2 + k_3\left(\frac{\sigma}{d}\right)^3\right), \tag{38}$$

with

$$\begin{aligned} k_0 &= -\ln(1-\eta) + \frac{(42\eta - 39\eta^2 + 9\eta^3 - 2\eta^4)}{6(1-\eta)^3}, \\ k_1 &= \frac{\eta^4 + 6\eta^2 - 12\eta}{2(1-\eta)^3}, \\ k_2 &= \frac{-3\eta^2}{8(1-\eta)^2}, \\ k_3 &= \frac{-\eta^4 + 3\eta^2 + 3\eta}{6(1-\eta)^3}. \end{aligned} \tag{39}$$

Any improvements to TPT1-E with respect to TPT1 are thereby lost because TPT1-E was developed from TPT1 by modifying Eq. (11). It might be that an analog of the TPT-E of Sec. II E can be developed starting from Eq. (38), but we do not pursue this in this paper.

We note that the MSPT should not be used for $\sigma/d(T) > \sqrt{2}$. For BH chains, this comes down to a maximum temperature of $k_BT/\epsilon = 447$ (ϵ being the well depth of the LJ potential), which is high enough for practical purposes.

For describing fluids at high densities and elevated temperatures, it is known that the leading-order approximation $A^{\mathrm{BHchain}} \approx A_d^{\mathrm{HSchain}}$ described above is not sufficiently accurate.[86,87] To improve the accuracy at those conditions, we add an (approximate) first-order Mayer-f perturbation contribution[88–90] to Eqs. (15) and (20) for describing the difference between the Helmholtz energy of a fluid of BH chains and a fluid comprising chains of hard spheres of diameter $d(T)$ bonded at $l = \sigma$. More details on this approach and an analytic implementation of this perturbation contribution are provided in Appendix C.

Applying the TPT-v model to BH chains further requires the second virial coefficient of two BH chains as input. We develop a model for this in Appendix D, based on a mapping onto the second virial coefficient of tangent hard-sphere chains.

III. RESULTS

A. Tangent, homo-segmented chains

In Fig. 4, we analyze the accuracy of TPT1, TPT1-v, TPT1-y, and TPT1-E in describing the pressure of tangent, homo-segmented hard-sphere chain fluids. The dataset of molecular simulation results

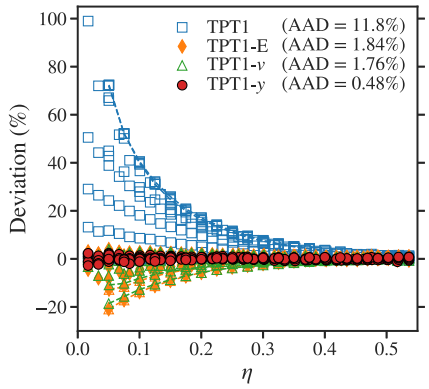

FIG. 4. Percentage deviation of TPT1, TPT-E, TPT1-v, and TPT1-y with respect to molecular simulation results for the residual pressure $p^{res} = p - p^{ig}$ (with $p^{ig} = \rho k_B T$) of homo-segmented tangent hard-sphere chain fluids comprising between two and 500 hard spheres per molecule.[35,61,77] Lines act as a guide for the eye for chains of 201 and 500 segments.

used for the analysis comprises the MC and MD data of Zmpitas and Gross[35] ($s = \{2, 4, 8, 16, 64\}$), the MD data of Jover *et al.*[77] ($s = \{16, 20, 100, 201, 500\}$), and the MC data of Rehner *et al.* ($s = 3$).[61] The complete dataset is provided in the supplementary material.

Compared to TPT1, all three low-density corrections developed in this work provide a significant improvement in the description of the pressure of homo-segmented tangent hard-sphere chain fluids. TPT1-y is the most accurate model, leading to an AAD = 0.48% and a Max-AD = 2.8%, as compared to an AAD = 11.8% and a Max-AD = 100% for TPT1. Second place is for TPT1-v with an AAD = 1.76% and Max-AD = 18.6%, followed by TPT1-E with an AAD = 1.84% and Max-AD = 20.9%. The superior description obtained based on TPT1-y is not surprising, since TPT1-y is the only model that was parameterized for the dataset shown in Fig. 4.

The similar performance of TPT-v and TPT-E can be ascribed to the fact that these models were both developed to reproduce the second virial coefficient. The results for the longest chains considered ($s = 201$ and $s = 500$; the largest negative deviations shown in Fig. 4) suggest such simple second-virial corrections cannot lead to a quantitative description of the equation of state of very long chain molecules over the whole range of fluid density. The reason for this might lie in the underestimation[66] of the third virial coefficient $B_3 = \partial^2 Z/\partial\rho^2|_{\rho=0}$ (and the fourth virial coefficient) by TPT1, which is not fully corrected for by either TPT1-v or TPT1-E. As an example, let us analyze the contribution of the TPT-v correction term of Eq. (15) to the third virial coefficient, which equals $-\tilde{V}_m(\tilde{B}_2 - B_2^{\mathrm{TPT1}}) > 0$, where $\tilde{V}_m$ is the average molecular volume of the mixture. Although this correction is of the right sign, its magnitude is too small: for homo-segmented tangent hard-sphere chains of $s = 100$, the correction only compensates for about 10% of the underestimation of B_3 by TPT1.[66]

The description of the second virial coefficient is analyzed in Fig. 2. An important observation is the slight deterioration in the TPT1-y description of B_2 for chains of more than, say, 50 segments. This is caused by the fact that TPT1-y is unable to alter the asymptotic scaling $B_2 \sim s^2$ of TPT1. The success of TPT1-y in describing the equation of state of very long chain molecules as shown in Fig. 4 then partly lies in this (incorrect) asymptotic scaling $B_2 \sim s^2$: apparently the accompanying overestimation of B_2 can sufficiently compensate for the underestimation of B_3 of long chains.

With the above in mind, we develop an alternative implementation of TPT1-v by multiplying the term $\exp(-\eta)(\tilde{B}_2 - \tilde{B}_2^{\mathrm{TPT1}})\rho$ of Eq. (15) by the following activation function of the average number of segments per chain molecule:

$$g(\tilde{s}) = \left(1.0 - \sqrt{\frac{a_0 \tilde{s}^2}{1 + a_1 \tilde{s}^2}}\right), \tag{40}$$

with $a_0 = 8.4803 \times 10^{-7}$ and $a_1 = 1.3235 \times 10^{-5}$. For chains of less than about 50 segments, the activation function is very close to unity, while for $s \to \infty$, it goes to a lower value of about 0.75. The description of the dataset in Fig. 4 thereby becomes of similar quality as that obtained by TPT1-y (AAD = 0.96%, Max-AD = 4.5%), while the asymptotic scaling of the second virial coefficient $B_2 \sim s^{1.75}$ is altered to $B_2 \sim s^2$. At this point, it is difficult to say whether this modification will be beneficial for describing real (polymeric) fluids; it is simply not clear what is more important for the success of a perturbation theory of chain fluids with attractive interactions: having the correct polymer scaling for B_2 of the repulsive reference fluid or having an accurate description of the pressure of this reference fluid. In the remainder of this paper, we only analyze the (unmodified) TPT1-v of Sec. II C.

B. Transferability to fused chains, hetero-segmented chains, and mixtures

Since all three low-density corrections developed in this work in some way incorporated molecular-simulation data for pure, homo-segmented tangent hard-sphere chain fluids, a key performance indicator of TPT1-v, TPT1-y, and TPT1-E is the transferability to fused chains, hetero-segmented chains, and mixtures. In Fig. 5, we analyze this transferability by comparing to newly generated NpT-MC simulation data for chains of $s = 10$ and $s = 20$ segments. The simulation details are listed in Appendix E, and the simulation results are tabulated in the supplementary material.

In Fig. 5(a), we first analyze the description of fused, homo-segmented chains of bond length $l^* = \{1.0, 0.8, 0.6\}$. The overestimation of the pressure by TPT1 is qualitatively similar for all bond lengths, although the absolute overestimation decreases with l^*. This is in agreement with our discussion of second virial coefficients in Sec. II B, where this effect was anticipated. TPT1 thus seems to be a better model for describing fused (less flexible) chains as compared to tangent (fully flexible) chains. Based on the data analyzed here, all three models developed in this work seem well transferable to fused chains, leading to a significant improvement with respect to TPT1.

Tangent, hetero-segmented chain fluids are analyzed in Fig. 5(b). Two types of hetero-segmented chains are considered: block-copolymer (BC) chains, consisting of a chain of $s/2$ segments with diameter $d_A = 1$, connected to a chain of $s/2$ segments of diameter $d_B > d_A$, and alternating (A) chains, where segments of types

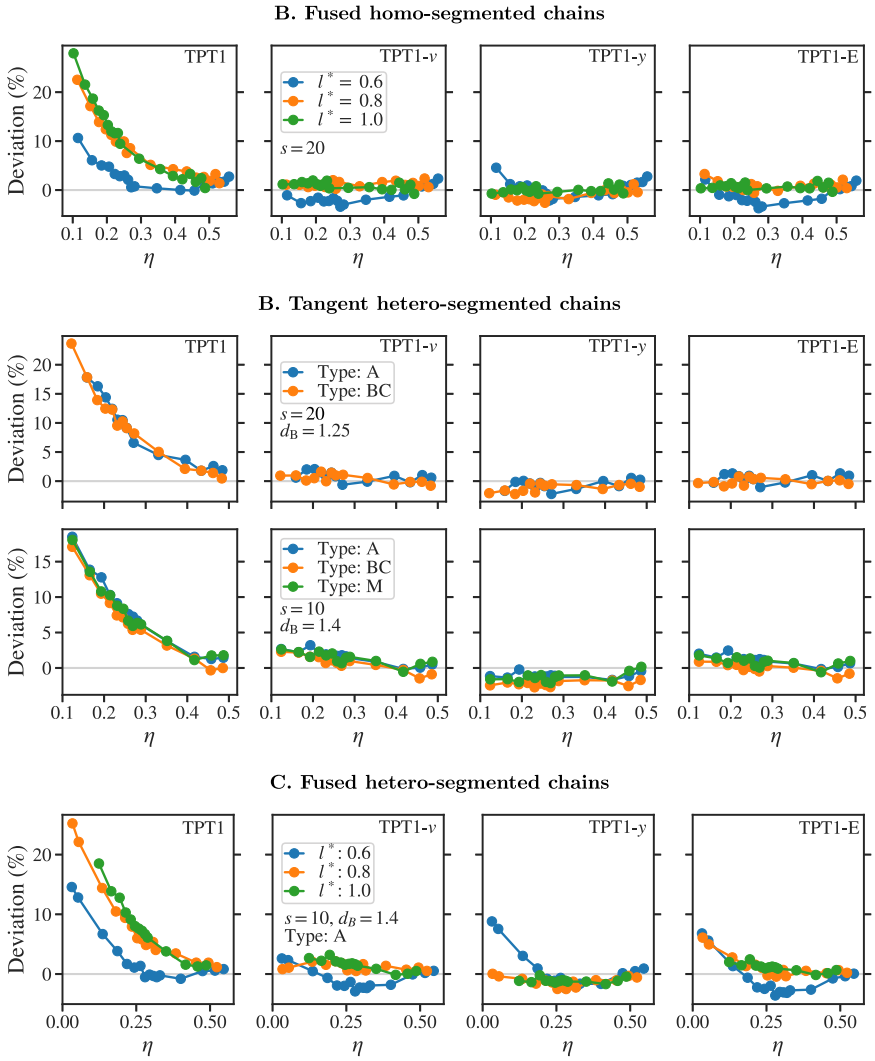

FIG. 5. Percentage deviations of TPT1, TPT1-v, TPT1-y, and TPT1-E with respect to molecular simulation data for the residual pressure $p^{res} = p - p^{ig}$ of (a) fused homo-segmented hard-sphere chains of 20 segments, (b) tangent hetero-segmented hard-sphere chains of 10 and 20 segments, and (c) fused hetero-segmented hard-sphere chains of 10 segments. Type BC denotes a block-copolymer with $s/2$ segments of diameter $d_A = 1$, followed by $s/2$ segments of diameter d_B; type A denotes a chain of alternating type A and type B segments; and type M denotes an equimolar mixture of chains with type A segments and chains with type B segments.

A and B alternate along the chain's backbone. Both $d_B = 1.25$ and $d_B = 1.4$ are analyzed. Our simulation results indicate that the pressure of hetero-segmented chain fluids is rather insensitive to the order of the segments along the chain's backbone. The transferability of TPT1-y, TPT1-v, and TPT1-E to tangent hetero-segmented chains seems excellent.

In the bottom diagram of Fig. 5(b), we also analyze an equimolar mixture (M) of chains of type 1, with segment diameter d_A, and chains of type 2, with segment diameter d_B. Again, the transferability of TPT1-y, TPT1-v, and TPT1-E is excellent. Interestingly, the pressure of this mixture is nearly identical to that of the hetero-segmented chains considered previously. This suggests that, for a given mole fraction of segments within a system, the pressure is rather invariant on how these segments are distributed within and among chains. Our MC simulation data for the respective second virial coefficient of the hard-sphere chains analyzed in this section (Table I) corroborates this finding.

Since the hard-sphere contribution to the Helmholtz energy is the same for all considered chain types (A, BC, and M), the Helmholtz energy contribution due to bonding (which is purely entropic for the hard chains considered here) must be invariant on the distribution of segments as well. Assuming this Helmholtz energy contribution can be described based on TPT1, this suggests $\ln g^{HS}_{AB}(d_{AB}) \approx \frac{1}{2}\left(\ln g^{HS}_{AA}(d_A) + \ln g^{HS}_{BB}(d_B)\right)$, which implies the fol-

lowing approximation for the contact value of the cavity-correlation function of hard spheres of type A and B,

$$g_{AB}^{\mathrm{HS}}(d_{\mathrm{AB}}) \approx \sqrt{g_{AA}^{\mathrm{HS}}(d_{\mathrm{A}})g_{BB}^{\mathrm{HS}}(d_{\mathrm{B}})}. \tag{41}$$

The accuracy of this approximation is easily tested using the BMCSL EOS result for the cavity-correlation function of two hard spheres at contact. We find that, for the ratio $d_{\mathrm{B}}/d_{\mathrm{A}} = 1.4$ considered in this section, the above approximation is accurate to within 3% for $\eta \leq 0.5$, with the largest deviation being observed for $\eta = 0.5$. This accuracy holds for ratios of $d_{\mathrm{B}}/d_{\mathrm{A}}$ all the way up to 2. The accuracy of the above approximation suggests that the pressure of tangent hetero-segmented hard-sphere chain mixtures is largely determined by the packing fraction and the segment mole fractions in the system. Further details of the mixture (e.g., the chain lengths of the different components in a mixture or the distribution of segments within and among chains) are much less important. We expect this to hold only for isotropic phases; for describing non-isotropic phases (e.g., self-assembled structures[91] or liquid crystals), such details definitely need to be taken into account.

The description of fused, hetero-segmented chain fluids is analyzed in Fig. 5(c). The chain molecules comprise 10 segments of type A and type B ($d_{\mathrm{A}} = 1$ and $d_{\mathrm{B}} = 1.4$) in alternating order. As for the other cases analyzed so far, all models developed in this work significantly improve on TPT1. However, the distinction between different models is more pronounced in this case, with TPT1-v leading to a better description of the simulation data as compared to TPT1-y and TPT1-E. The good transferability of TPT1-v is probably caused by having the exact second virial coefficient as input. TPT1-y and TPT1-E require no such input and, thus, can be considered fully predictive. With that in mind, the results of those models are considered very satisfactory.

So far, we have only focused on the description of chain fluids with a considerable number of segments per molecule ($s = 10$ or $s = 20$). This is for the simple reason that the low-density corrections developed in this work are more significant for longer chains, where the low-density description obtained from TPT1 becomes inaccurate. It is also important, however, to analyze whether the rather accurate TPT1 description of chain fluids with only a small number of segments per molecule is not compromised by our low-density corrections. We, therefore, compare theoretical predictions to molecular simulation results[61] for several hetero-nuclear (fused) hard trimers in Fig. 6 (please see the supplementary material for the complete dataset of molecular simulation results used for this analysis). It is rewarding to see that TPT1-y and TPT1-E do not deteriorate the description as compared to TPT1, but instead slightly improve on it. We expect similar results for TPT-v because the second virial coefficient of trimers as predicted by TPT1 is very similar to the exact second virial coefficient used as input for TPT-v. There will thus be little difference between the predictions of those models for the trimers shown in Fig. 6.

C. Chains of soft-repulsive (BH) segments

To appreciate the modifications made to arrive at the TPT1 for BH chains in Sec. II F, we first analyze the description of BH dimers. We do this for three different implementations of TPT1:

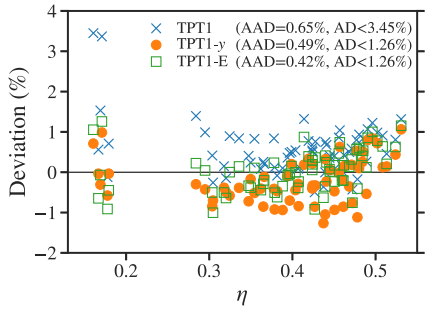

FIG. 6. Percentage deviation of TPT1, TPT1-y, and TPT1-E with respect to molecular simulation data[61] for the residual pressure of heteronuclear (fused) hard trimers. The data comprises trimers 5–10 from Table I of Rehner *et al.*[61]

(1) a TPT1 where the bond-length is (erroneously) set to the hard-sphere diameter $l = d(T)$, (2) a TPT1 where the bond-length is fixed at its actual value $l = \sigma$, and (3) the same, but with the Mayer-f perturbation contribution from Appendix C for describing the effects of soft repulsive intermolecular interactions included. The respective predictions for the pressure at various dimensionless temperatures $T^* = \{2, 3, 4, \ldots, 20\}$ are compared to the grand-canonical MC simulation data of van Westen *et al.*[73] in Fig. 7.

The comparison of case (2) to (1) shows the merit of having a model that allows a decoupling between the effects of bond-length and hard-sphere diameter on the Helmoltz-energy contribution of chain formation. When the bond-length remains fixed at its value $l = \sigma$ instead of (erroneously) changing with the hard-sphere diameter $d(T)$, the description of the low- and medium-density regimes improves significantly. We emphasize that decoupling bond-length and hard-sphere diameter is a feature of TPT1, which gives one the freedom to use the MSPT model from Eq. (38) for the cavity-correlation function of hard spheres at distances beyond d.

At high densities, the TPT1 of case (2) overestimates the pressure, an effect that becomes stronger at higher temperatures. This is a known effect,[73,86,87] caused by an insufficient description of the decrease in pressure due to the soft (rather than hard) repulsive interactions between molecules. Comparing case (3) with (2)

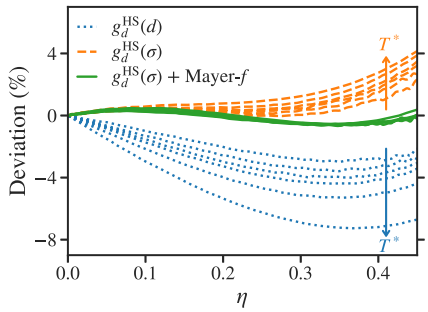

FIG. 7. Percentage deviation of several implementations of TPT1 with respect to molecular simulation data[73] for the total pressure of BH dimer fluids at temperatures $T^* = \{2, 3, 4, 5, 8, 20\}$.

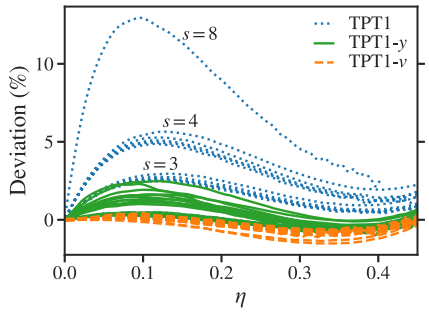

FIG. 8. Percentage deviation of TPT1, TPT1-y, and TPT1-v with respect to molecular simulation data[73] for the total pressure of BH chain fluids of $s = \{2, 3, 4, 8\}$ and temperatures within the range $T^* = [2, 20]$.

shows that including the Mayer-f perturbation contribution cancels much of the inaccuracies observed for case (2), leading to a near-quantitative description of BH dimers.

In the remainder of this section, the classification "TPT1" strictly applies to the model from Sec. II F. That is, a TPT1 where the cavity-correlation function is evaluated for a distance equal to the bond length $l = \sigma$ and with the Mayer-f perturbation contribution for describing soft-repulsive interactions included.

The description of BH trimers, 4-mers, and 8-mers is analyzed in Fig. 8. The deviations of TPT1 with respect to molecular-simulation data resemble those of hard-sphere chains (cf. Fig. 4), suggesting the low-density corrections of TPT-v and TPT-y are well transferable. We consider the results of TPT-y to be especially pleasing because TPT-y is fully predictive for BH chains, requiring no external input from molecular simulations. This means that TPT1-y can be applied on the fly to describe BH chains for other (target) intermolecular potentials than the Lennard-Jones potential considered here; all that is required for this is replacing the Lennard-Jones potential by the potential of interest in the integral of Eq. (37) for the hard-sphere diameter. For generalized Lennard-Jones (Mie) potentials, the model provided in Appendix B calculates this integral analytically.[84] Applying TPT-v to BH-Mie chains would instead require a model for the second virial coefficient of these chains, which (for now) is not available.

IV. CONCLUSION

The three low-density corrections to TPT1 developed in this work, namely, TPT1-v, TPT1-y, and TPT1-E, lead to a significantly improved description of tangent homo-segmented hard-sphere chain fluids and exhibit excellent transferability to systems containing hetero-segmented chains, fused chains, and mixtures. Moreover, both TPT1-v and TPT1-y can also effectively describe soft-repulsive (Barker–Henderson) chain fluids with satisfying accuracy. Despite being empirical, these low-density corrections thus possess a generic character, which is particularly advantageous for their utilization as part of a versatile equation-of-state model such as SAFT. Among the three models, TPT1-y stands out as the most generic, as it can be applied predictively to all chain types analyzed in this work without relying on external input from molecular simulations. When describing Barker–Henderson chains for a generalized Lennard-Jones (Mie) target potential between chain segments, TPT1-y can be readily employed using the hard-sphere diameter from Appendix B. The results obtained for fused hetero-segmented chains indicate that TPT1-v demonstrates superior transferability. However, TPT1-v is less generic due to its dependence on the second virial coefficient of chain fluids, which may not be readily available. It would be interesting to further investigate the transferability of these equation-of-state models for describing branched chains or chains with intramolecular potentials such as bond-bending and torsion. The extension of TPT1-y to describe such chains could be pursued based on previous work,[41] while TPT1-v would require the availability of a suitable model for the second virial coefficient of such chains. A further distinction between TPT1-v, TPT1-y, and TPT1-E could be explored through their application as functionals in classical density functional theory for describing inhomogeneous chain fluids, including interfaces[91] and fluids confined in porous solids.[92] It would also be interesting to analyze to what degree the approaches developed in this work can be generalized to chain molecules with attractive intermolecular interactions.

SUPPLEMENTARY MATERIAL

We refer to the online supplementary material for data files containing the results of all molecular simulations performed in this work and all molecular simulation results from the literature that were used in this work.

ACKNOWLEDGMENTS

The authors gratefully acknowledge Wasilios Zmpitas for proposing the TPT-v approach. T.v.W. and J.G. thank the German Research Foundation (DFG) for the financial support within the Cluster of Excellence in Simulation Technology (Grant No. EXC 2075, Project ID No. 390740016) at the University of Stuttgart. The authors also acknowledge the computational time spent on the BwUniCluster within the framework program bwHPC. P.R. acknowledges the funding by the Deutsche Forschungsgemeinschaft (DFG, German Research Foundation)—Grant No. 497566159.

AUTHOR DECLARATIONS

Conflict of Interest

The authors have no conflicts to disclose.

Author Contributions

Thijs van Westen: Conceptualization (equal); Investigation (equal); Software (equal); Writing – original draft (equal); Writing – review & editing (equal). **Philipp Rehner**: Conceptualization (equal); Investigation (equal); Software (equal); Writing – original draft (equal); Writing – review & editing (equal). **Thijs J. H. Vlugt**: Conceptualization (equal); Investigation (equal); Software (equal); Writing – original draft (equal); Writing – review & editing

(equal). **Joachim Gross**: Conceptualization (equal); Investigation (equal); Software (equal); Writing – original draft (equal); Writing – review & editing (equal).

DATA AVAILABILITY

The data that supports the findings of this study are available within the article and its supplementary material.

APPENDIX A: ANALYTIC SECOND VIRIAL COEFFICIENT OF FULLY FLEXIBLE, TANGENT HARD-SPHERE CHAINS

The second virial coefficient of fully flexible tangent hard-sphere chain (THSC) molecules is described using

$$\frac{B_2^{\mathrm{THSC}}}{V_m} = \frac{11s-3}{2s} + 1.4535\frac{(s-1)^{2-\gamma}}{s}, \tag{A1}$$

where $V_m = (\pi/6)sd^3$ is the molecular volume. The parameter γ was correlated to the MC simulation data for B_2 of Yethiraj *et al.*[67] and Vega *et al.*,[66] which comprises chain lengths ranging from $s = 3$ up to $s = 200$ (see the supplementary material for the complete dataset). Following the analysis of Yethiraj *et al.*,[67] we add a small chain-length dependence in the exponent, leading to

$$\gamma = 0.2079 + \frac{0.6388}{s^3}, \tag{A2}$$

which describes the complete dataset with an AAD of 0.7% and a Max-AD of 1.7% ($s = 200$). The asymptotic value $\gamma = 0.2079$ for $s \to \infty$ is in reasonable agreement with available predictions from theoretical and simulation approaches, $\gamma \approx [0.2, 0.25]$ (see Yethiraj *et al.*[67] and references therein). For dimers, or $\gamma = 0$, Eq. (A1) reduces to the model for rigid-linear tangent hard-sphere chains of Jaffer *et al.*[76] and [to within 0.016% of the term of order $(s-1)^2$] the model of Williamson and Jackson.[75]

APPENDIX B: HARD-SPHERE DIAMETER FOR DESCRIBING SOFT REPULSIVE BH SEGMENTS

As shown by van Westen and Gross,[84] the integral of Eq. (37) is accurately described using the following parametric equation in terms of the dimensionless temperature $T^* = kT/\epsilon$ (where ϵ is the well depth of the LJ potential), the LJ size parameter σ, and the repulsive exponent ν of a Mie $\nu-6$ potential (which equals 12 for the LJ potential considered here),

$$\frac{d(T^*,\nu)}{\sigma} = \left[1 + C_0T^* + \ln(1+T^*)\sum_{k=1}^{3} C_iT^{*\frac{2k-1}{4}} + C_4T^{*2}\right]^{-\frac{1}{2\nu}}, \tag{B1}$$

where C_0 is determined by the exact asymptotic low-temperature scaling of Eq. (37),

$$C_0 = -\frac{2\nu}{(n-\nu)\mathcal{C}}, \tag{B2}$$

with

$$\mathcal{C} = \frac{\nu}{\nu-6}\left(\frac{\nu}{6}\right)^{\frac{6}{\nu-6}}, \tag{B3}$$

TABLE III. Correlated constants c_i for the hard-sphere diameter d of Eq. (B1). The maximum absolute deviations (denoted by ϵ) of the hard-sphere diameter d, its temperature derivative d', the second virial coefficient of the reference fluid $B_{20} = (2/3)\pi d^3$, and its temperature derivative B'_{20}, are given at the bottom of the table. These deviations are for a range in temperature $0 \le T^* \le 25$ and repulsive Mie exponent $7 \le m \le 80$.[84]

c_1	$1.09\,360\,455\,168\,912 \times 10^{-2}$
c_2	$-2.00\,897\,880\,971\,934 \times 10^{-1}$
c_3	$-1.27\,074\,910\,870\,683 \times 10^{-2}$
c_4	$1.40\,422\,470\,174\,053 \times 10^{-2}$
c_5	$7.35\,946\,850\,956\,932 \times 10^{-2}$
c_6	$1.28\,463\,973\,950\,737 \times 10^{-2}$
c_7	$3.71\,527\,116\,894\,441 \times 10^{-3}$
c_8	$5.05\,384\,813\,757\,953 \times 10^{-3}$
c_9	$4.91\,003\,312\,452\,622 \times 10^{-2}$
$\epsilon(d)$	9.95×10^{-5}
$\epsilon(d')$	5.18×10^{-4}
$\epsilon(B_{20})$	5.72×10^{-4}
$\epsilon(B'_{20})$	3.26×10^{-3}

defining the pre-factor of the Mie $\nu-6$ pair potential. The remaining coefficients are calculated as

$$\begin{pmatrix} C_1 \\ C_2 \\ C_3 \\ C_4 \end{pmatrix} = \begin{pmatrix} c_1 & & \\ c_2 & c_3 & \\ c_4 & c_5 & c_6 \\ c_7 & c_8 & c_9 \end{pmatrix} \begin{pmatrix} 1 \\ \alpha' \\ \alpha'^2 \end{pmatrix}, \tag{B4}$$

with

$$\alpha' = \frac{1}{\alpha_{\nu 6}(1)} - \frac{1}{\alpha_{76}(1)}, \tag{B5}$$

and $\alpha_{\nu 6}(x)$ denoting the dimensionless mean-field constant,

$$\begin{aligned}\alpha_{\nu 6}(x) &= -\int_x^\infty u^*(r^*)r^{*2}\mathrm{d}r^* \\ &= \mathcal{C}\left(\frac{x^{-3}}{3} - \frac{x^{3-\nu}}{\nu-3}\right).\end{aligned} \tag{B6}$$

The constants $(c_i,\ i = (1,\ldots,9))$ and some details on the accuracy and range of validity of this correlation are listed in Table III.

APPENDIX C: FIRST-ORDER MAYER-f PERTURBATION CONTRIBUTION FOR THE DIFFERENCE BETWEEN BH CHAINS AND HARD-SPHERE CHAINS

The difference between the Helmholtz energy of a fluid of BH monomers and a fluid of hard spheres of effective diameter $d(T)$ can be expanded in a perturbation series using a Mayer-f expansion.[88–90] The first-order perturbation term is written as

$$\tilde{a}^{\mathrm{BH}} - \tilde{a}_d^{\mathrm{HS}} = -2\pi\rho\int_0^\sigma y_d^{\mathrm{HS}}(r)\Delta e(r)r^2\mathrm{d}r, \tag{C1}$$

where $\Delta e(r) = \exp(-\beta u^{\mathrm{LJ}}(r)) - \exp(-\beta u^{\mathrm{HS}}(r))$. The above integral is calculated using the analytic implementation provided in the supplementary material of van Westen and Gross.[69]

For describing the difference between the Helmholtz energy of a fluid of BH chains (BHCH) and a fluid comprising chains of hard spheres of diameter $d(T)$ bonded at a distance $l = \sigma$ (HSCH), the above perturbation contribution should be modified. Here, we do this in a rather crude manner, as follows:

$$\tilde{a}^{\mathrm{BHCH}} - \tilde{a}_d^{\mathrm{HSCH}} \approx s\frac{\tilde{a}^{\mathrm{BH}} - \tilde{a}_d^{\mathrm{HS}}}{2 - \frac{1}{s}}, \tag{C2}$$

which can simply be added to Eqs. (15) and (20) to describe the effects of soft repulsion between BH chains.

The pre-factor of Eq. (C2) accounts for the trivial multiplication with s to render a perturbation contribution per molecule rather than per segment. The division by $2 - 1/s$ scales down the perturbation term of monomers when the number of segments per chain increases. The perturbation term of monomers is scaled down by at most a factor of 1/2 for $s \to \infty$. Scaling down the perturbation term for $s > 1$ is done based on the empirical observation that adding Eq. (C1) (multiplied by s) to Eqs. (15) and (20) leads to a slight underestimation of the pressure of BH chains at high densities. This underestimation might be caused by the fact that we neglect the Mayer-f perturbation contribution for the difference between the cavity-correlation function of BH monomers and hard spheres in describing the TPT1 contribution to chain formation in Eq. (1).[87]

APPENDIX D: SECOND VIRIAL COEFFICIENT OF BARKER–HENDERSON CHAINS

We map the second virial coefficient of BH chain (BHC) molecules onto that of tangent hard-sphere chain (THSC) molecules, using

$$B_2^{\mathrm{BHC}} = B_2^{\mathrm{THSC}}\left(\frac{d_{\mathrm{eff}}(T^*, s)}{\sigma}\right)^3, \tag{D1}$$

with the effective hard-sphere diameter,

$$\frac{d_{\mathrm{eff}}(T^*, s)}{\sigma} = \left(\frac{1}{1 + C_1 T^* + C_2 T^{*2}}\right)^{\frac{1}{24}C_3}, \tag{D2}$$

and

$$C_i(T, s) = c_{i0} + c_{i1}\left(\frac{s-1}{s}\right) + c_{i2}\left(\frac{s-1}{s}\right)\left(\frac{s-2}{s}\right) \tag{D3}$$

for $i \in [1, 2, 3]$. The nine model constants c_{ij} were used to correlate MC simulation results for the second virial coefficient of BH chains by van Westen *et al.*[73] The range in the number of segments and temperatures considered is $s = [1, 2, 3, 5, 8, 16, 32]$ and $T^* = [0.7, 1, 1.5, 2, 3, 5, 7, 10, 20]$. The full dataset is provided in the supplementary material of this work. The adjusted constants are listed in Table IV.

APPENDIX E: SIMULATION DETAILS

1. MC simulations of second virial coefficients

The second virial coefficient of two chain molecules 1 and 2 of intermolecular potential energy U_{12} is defined as

$$B_2 = -2\pi \int \left(\langle \exp\left(-\beta U_{12}(r, \Omega_1, \Omega_2)\right)\rangle_{\Omega_1\Omega_2} - 1\right) r^2 \mathrm{d}r, \tag{E1}$$

where r is the distance between the centers of mass of chains 1 and 2, and Ω is a vector describing the full configuration of a chain (e.g., the orientation vector of one bond and the total set of bond and torsion angles). The ensemble average $\langle \cdots \rangle_{\Omega_1\Omega_2}$ was sampled over a grid in the intermolecular distance $r^* = r/\sigma = [0, r^*_{\mathrm{max}}]$, along ten random directions $\hat{\boldsymbol{r}} = \boldsymbol{r}/r$, for 10^5 independent chain pairs and 40 random relative orientations of the chains. The configurations of the chains were generated independently using the Rosenbluth method.[93–96] To remove the bias introduced by the Rosenbluth method and to recover Boltzmann statistics, each chain pair was given a statistical weight equal to the product of the individual Rosenbluth weights of chains 1 and 2. Different relative orientations of chains 1 and 2 were generated by rotating chain 2 (in particular, the vector pointing to its center of mass and the vectors describing the relative positions of the segments with respect to the center of mass) with respect to a randomly chosen (x, y, or z) axis of the Cartesian reference frame. The maximum grid-distance r^*_{max} was set to the sum of the maximum lengths of chain 1 and 2 (i.e., the length in an extended, linear configuration), and we used a grid spacing $\Delta r^* = 0.05$. Results for the second virial coefficient were averaged over at least five independent calculations, and the statistical uncertainty was estimated as the root-mean-square deviation of these independent calculations with respect to their average.

2. *NpT*-MC simulations

The density of hard-sphere chain fluids was calculated for a specified pressure p^* by isobaric–isothermal NpT-MC simulations[96] performed using an in-house MC code. The code was validated in previous work.[61] Fused chains were handled by replacing the hard-sphere potential for next-nearest neighbors α and α''

TABLE IV. Correlated constants c_{ij} of Eq. (D3).

j	1	2	3
i			
1	0.852 987 920 795 915	−0.128 229 846 701 676	0.833 664 689 185 409
2	0.024 047 779 523 804 5	0.017 761 832 199 916 4	0.127 015 906 854 396
3	1	−0.528 941 139 160 234	−0.147 289 922 797 747

within a chain molecule with a hard-angle potential. The hard-angle potential changes from zero to infinity only when these segments overlap outside segment α', prohibiting the rejection of viable configurations where segments α and α'' overlap within segment α' (see Fig. 3). We refer to Rehner *et al.*[61] for further details. We used a cubic box with periodic boundary conditions, containing between N_s = 1500 and N_s = 2000 segments. We employed at least 10^6 MC cycles for equilibration and 10^6 cycles for production, with each cycle comprising N MC moves. The MC moves considered were translation,[96] rotation,[96] configurational bias regrowth,[97,98] crank-shaft moves,[31,99] and volume moves,[96] with relative probabilities of 0.286, 0.286, 0.129, 0.286, 0.0143 (10-mers) and 0.22, 0.22, 0.1, 0.44, 0.011 (20-mers). During equilibration, the step-size for translation, rotation, and volume moves was adjusted to obtain ~20% acceptance. For the configurational bias regrowth move, we chose a random segment as the starting segment and regrew the molecule in a random direction (forward or backward) using six trial orientations for each new segment. The crank-shaft moves were combined with a configurational bias scheme, using six trial angles for the rotated segment. The statistical uncertainty of the sampled density was estimated by dividing the production part of the simulation into five blocks and calculating the standard deviation of the block averages with respect to the average over all five blocks.

REFERENCES

[1] S. Beret and J. M. Prausnitz, AIChE J. **21**, 1123 (1975).
[2] M. D. Donohue and J. M. Prausnitz, AIChE J. **24**, 849 (1978).
[3] G. Jackson, W. G. Chapman, and K. E. Gubbins, Mol. Phys. **65**, 1 (1988).
[4] W. G. Chapman, G. Jackson, and K. E. Gubbins, Mol. Phys. **65**, 1057 (1988).
[5] W. G. Chapman, K. E. Gubbins, G. Jackson, and M. Radosz, Ind. Eng. Chem. Res. **29**, 1709 (1990).
[6] A. Gil-Villegas, A. Galindo, P. J. Whitehead, S. J. Mills, G. Jackson, and A. N. Burgess, J. Chem. Phys. **106**, 4168 (1997).
[7] J. Gross and G. Sadowski, Ind. Eng. Chem. Res. **40**, 1244 (2001).
[8] T. Lafitte, D. Bessieres, M. M. Piñeiro, and J. Daridon, J. Chem. Phys. **124**, 024509 (2006).
[9] T. Lafitte, A. Apostolakou, C. Avendãno, A. Galindo, C. S. Adjiman, E. A. Müller, and G. Jackson, J. Chem. Phys. **139**, 154504 (2013).
[10] E. A. Müller and K. E. Gubbins, Ind. Eng. Chem. Res. **40**, 2193 (2001).
[11] I. G. Economou, Ind. Eng. Chem. Res. **41**, 953 (2002).
[12] P. Paricaud, A. Galindo, and G. Jackson, Fluid Phase Equilib. **194–197**, 87 (2002).
[13] S. P. Tan, H. Adidharma, and M. Radosz, Ind. Eng. Chem. Res. **47**, 8063 (2008).
[14] C. McCabe and A. Galindo, in *Applied Thermodynamics of Fluids*, edited by A. R. H. Goodwin, J. V. Sengers, and C. J. Peters (The Royal Society of Chemistry, Cambridge, 2010) Chap. 8, pp. 215–279.
[15] K. S. Schweizer and J. G. Curro, J. Chem. Phys. **89**, 3350 (1988).
[16] Y. C. Chiew, Mol. Phys. **70**, 129 (1990).
[17] V. S. Mitlin and I. C. Sanchez, J. Chem. Phys. **99**, 533 (1993).
[18] Y. Song, S. M. Lambert, and J. M. Prausnitz, Macromolecules **27**, 441 (1994).
[19] G. Stell, C.-T. Lin, and Y. V. Kalyuzhnyi, J. Chem. Phys. **110**, 5444 (1999).
[20] G. Stell, C.-T. Lin, and Y. V. Kalyuzhnyi, J. Chem. Phys. **110**, 5458 (1999).
[21] C.-T. Lin, G. Stell, and Y. V. Kalyuzhnyi, J. Chem. Phys. **112**, 3071 (2000).
[22] P. Attard, J. Chem. Phys. **102**, 5411 (1995).
[23] M. P. Taylor and J. E. G. Lipson, J. Chem. Phys. **102**, 6272 (1995).
[24] H. H. Gan and B. C. Eu, J. Chem. Phys. **105**, 4323 (1996).
[25] M. S. Wertheim, J. Stat. Phys. **42**, 477 (1986).
[26] M. S. Wertheim, J. Chem. Phys. **87**, 7323 (1987).
[27] S. Phan, E. Kierlik, M. L. Rosinberg, H. Yu, and G. Stell, J. Chem. Phys. **99**, 5326 (1993).
[28] E. A. Müller and K. E. Gubbins, Mol. Phys. **80**, 957 (1993).
[29] D. Ghonasgi and W. G. Chapman, J. Chem. Phys. **100**, 6633 (1994).
[30] J. Chang and S. I. Sandler, Chem. Eng. Sci. **49**, 2777 (1994).
[31] F. A. Escobedo and J. J. de Pablo, J. Chem. Phys. **102**, 2636 (1995).
[32] K. P. Shukla and W. G. Chapman, Mol. Phys. **91**, 1075 (1997).
[33] K. P. Shukla and W. G. Chapman, Mol. Phys. **98**, 2045 (2000).
[34] B. D. Marshall and W. G. Chapman, J. Chem. Phys. **138**, 174109 (2013).
[35] W. Zmpitas and J. Gross, Fluid Phase Equilib. **416**, 18 (2016).
[36] B. D. Marshall, J. Chem. Phys. **144**, 164104 (2016).
[37] W. Zmpitas and J. Gross, J. Chem. Phys. **150**, 244902 (2019).
[38] Y. Zhou and G. Stell, J. Chem. Phys. **96**, 1507 (1992).
[39] Y. Hu, H. Liu, and J. M. Prausnitz, J. Chem. Phys. **104**, 396 (1996).
[40] H. Liu and Y. Hu, Fluid Phase Equilib. **122**, 75 (1996).
[41] T. van Westen, B. Oyarzún, T. J. H. Vlugt, and J. Gross, Mol. Phys. **112**, 919 (2014).
[42] R. Dickman and C. K. Hall, J. Chem. Phys. **85**, 4108 (1986).
[43] R. Dickman and C. K. Hall, J. Chem. Phys. **89**, 3168 (1988).
[44] K. G. Honnell and C. K. Hall, J. Chem. Phys. **90**, 1841 (1989).
[45] M. A. Denlinger and C. K. Hall, Mol. Phys. **71**, 541 (1990).
[46] K. G. Honnell and C. K. Hall, J. Chem. Phys. **95**, 4481 (1991).
[47] A. Yethiraj and C. K. Hall, J. Chem. Phys. **94**, 3943 (1991).
[48] A. Yethiraj and C. K. Hall, Mol. Phys. **80**, 469 (1993).
[49] S. D. Mehta and K. G. Honnell, J. Phys. Chem. **100**, 10408 (1996).
[50] H. S. Gulati, J. M. Wichert, and C. K. Hall, J. Chem. Phys. **104**, 5220 (1996).
[51] T. Boublík, Mol. Phys. **68**, 191 (1989).
[52] T. Boublík, C. Vega, and M. Diaz-Penã, J. Chem. Phys. **93**, 730 (1990).
[53] A. L. Archer and G. Jackson, Mol. Phys. **73**, 881 (1991).
[54] M. D. Amos and G. Jackson, Mol. Phys. **74**, 191 (1991).
[55] F. J. Blas and L. F. Vega, J. Chem. Phys. **115**, 3906 (2001).
[56] J. M. Walsh and K. E. Gubbins, J. Phys. Chem. **94**, 5115 (1990).
[57] M. D. Amos and G. Jackson, J. Chem. Phys. **96**, 4604 (1992).
[58] S. Phan, E. Kierlik, and M. L. Rosinberg, J. Chem. Phys. **101**, 7997 (1994).
[59] Y. Zhou, C. K. Hall, and G. Stell, J. Chem. Phys. **103**, 2688 (1995).
[60] A. Dominik, P. Jain, and W. G. Chapman, Mol. Phys. **103**, 1387 (2005).
[61] P. Rehner, T. van Westen, and J. Gross, Phys. Rev. E **105**, 034110 (2022).
[62] E. Kierlik and M. L. Rosinberg, J. Chem. Phys. **99**, 3950 (1993).
[63] K. G. Honnell, J. G. Curro, and K. S. Schweizer, Macromolecules **23**, 3496 (1990).
[64] Y. C. Chiew, Mol. Phys. **73**, 359 (1991).
[65] F. A. Escobedo and J. J. de Pablo, J. Chem. Phys. **103**, 1946 (1995).
[66] C. Vega, J. M. Labaig, L. G. MacDowell, and E. Sanz, J. Chem. Phys. **113**, 10398 (2000).
[67] A. Yethiraj, K. G. Honnell, and C. K. Hall, Macromolecules **25**, 3979 (1992).
[68] T. van Westen and J. Gross, J. Chem. Phys. **154**, 041102 (2021).
[69] T. van Westen and J. Gross, J. Chem. Phys. **155**, 244501 (2021).
[70] J. R. Elliott, J. Phys. Chem. B **125**, 4494 (2021).
[71] T. Boublík, J. Chem. Phys. **53**, 471 (1970).
[72] G. Mansoori, N. F. Carnahan, K. E. Starling, and T. W. Leland, J. Chem. Phys. **54**, 1523 (1971).
[73] T. van Westen, T. J. H. Vlugt, and J. Gross, J. Chem. Phys. **142**, 224504 (2015).
[74] W. Zmpitas and J. Gross, Fluid Phase Equilib. **428**, 121 (2016).
[75] D. C. Williamson and G. Jackson, Mol. Phys. **86**, 819 (1995).
[76] K. M. Jaffer, S. B. Opps, and D. E. Sullivan, J. Chem. Phys. **110**, 11630 (1999).
[77] J. Jover, A. J. Haslam, A. Galindo, G. Jackson, and E. A. Müller, J. Chem. Phys. **137**, 144505 (2012).
[78] P. Attard and G. Stell, Chem. Phys. Lett. **189**, 128 (1992).
[79] W. Kuhn, Kolloid-Z. **87**, 3 (1939).
[80] H. Yamakaw, *Modern Theory of Polymer Solutions* (Harper & Row, New York, 1971).

[81] M. Rubinstein and R. H. Colby, *Polymer Physics* (Oxfor University Press, Oxford, 2003).
[82] J. A. Barker and D. Henderson, J. Chem. Phys. **47**, 4714 (1967).
[83] P. Paricaud, J. Chem. Phys. **124**, 154505 (2006).
[84] T. van Westen and J. Gross, J. Chem. Phys. **154**, 234502 (2021).
[85] T. Boublík, Mol. Phys. **59**, 775 (1986).
[86] T. van Westen and J. Gross, J. Chem. Phys. **147**, 014503 (2017).
[87] T. van Westen and J. Gross, Mol. Phys. **120**, e2059410 (2022).
[88] J. A. Barker, Proc. R. Soc. A **241**, 547 (1957).
[89] H. C. Andersen, J. D. Weeks, and D. Chandler, Phys. Rev. A **4**, 1597 (1971).
[90] K. E. Gubbins, W. R. Smith, M. K. Tham, and E. W. Tiepel, Mol. Phys. **22**, 1089 (1971).
[91] P. Rehner, B. Bursik, and J. Gross, Ind. Eng. Chem. Res. **60**, 7111 (2021).
[92] E. Sauer and J. Gross, Langmuir **35**, 11690 (2019).
[93] M. N. Rosenbluth and A. W. Rosenbluth, J. Chem. Phys. **23**, 356 (1955).
[94] D. Frenkel and B. Smit, Mol. Phys. **75**, 983 (1992).
[95] D. Frenkel, G. C. A. M. Mooij, and B. Smit, J. Phys.: Condens. Matter **4**, 3053 (1992).
[96] D. Frenkel and B. Smit, in *Understanding Molecular Simulation: From Algorithms to Applications*, 2nd ed. (Academic Press, San Diego, 2002).
[97] D. Frenkel, G. C. A. M. Mooij, and B. Smit, J. Phys.: Condens. Matter **3**, 3053 (1991).
[98] J. I. Siepmann and D. Frenkel, Mol. Phys. **75**, 59 (1992).
[99] X. Li and Y. C. Chiew, J. Chem. Phys. **101**, 2522 (1994).